Biosensors and Bioelectronics 47 (2013) 361–367

Contents lists available at SciVerse ScienceDirect

Biosensors and Bioelectronics

journal homepage: www.elsevier.com/locate/bios

A simple and rapid optical biosensor for detection of aflatoxin B1 based on competitive dispersion of gold nanorods

Xia Xu [a,b], Xiangjiang Liu [a,b], Yanbin Li [a,c], Yibin Ying [a,b,*]

[a] College of Biosystems Engineering and Food Science, Zhejiang University, Hangzhou 310058, PR China
[b] Key Laboratory of Equipment and Informatization in Environment Controlled Agriculture, Ministry of Agriculture, PR China
[c] Department of Biological & Agricultural Engineering, University of Arkansas, Fayetteville, AR 72701,USA

ARTICLE INFO

Article history:
Received 11 December 2012
Received in revised form
11 March 2013
Accepted 20 March 2013
Available online 29 March 2013

Keywords:
Aflatoxin B1
Gold nanorods
Optical Biosensor
Competitive immunoassay
Dispersion

ABSTRACT

This report illustrates a promising one-step and label-free optical biosensor for determination of aflatoxin B1 (AFB1) that is most commonly found in foods and highly dangerous even at very low concentrations. In this research, gold nanorods (GNRs) were employed as a sensing platform, which showed high stability under high ionic strength conditions without addition of any stabilizing agent. GNR-AFB1–BSA (bovine serum albumin) conjugates aggregated after mixing with free antibodies, resulting in significant changes in absorption intensity. At the same time the existence of AFB1 molecules in samples caused dispersion of nanorods, as a result of competitive immune-reaction with antibodies. By taking advantages of the competitive dispersion of GNRs, the developed method could effectively reduce false results caused by undesirable aggregation, which is a big problem for spherical gold nanoparticles. Absorption intensity of UV–vis spectra served as the sensing indicator, with dynamic light scattering (DLS) measurement as another sensing tool. The designed biosensing system could detect AFB1 in a linear range from 0.5 to 20 ng mL^{-1}, with a good correlation coefficient of 0.99. And the limit of detection (LOD) was 0.16 ng mL^{-1}, indicating an excellent sensitivity with absorbance result. The recoveries of the spiked AFB1 in real peanut samples ranged from 94.2% to 117.3%. Therefore the proposed nano-biosensor was demonstrated to be sensitive, selective, and simple, providing a viable alternative for rapid screening of toxins in agriculture products and foods.

1. Introduction

Aflatoxins (AFs) are naturally occurring mycotoxins produced by many species of *Aspergillus*, most notably *Aspergillus flavus* and *Aspergillus parasiticus* during the growth on foods and feeds (Williams et al., 2004). They are listed as group I carcinogens by the International Agency for Research on Cancer (IARC), primarily affecting liver (Lee et al., 2004). Although more than 20 AFs have been identified, the major AFs of concern are designated B1 (AFB1), B2, G1 and G2. And among them, AFB1 is normally predominant in amount and the most toxic (Delmulle et al., 2005; Zhang et al., 2009). As a result, many countries and regions in the world have regulatory limits for levels of AFB1 in agricultural products. Therein the European Commission has set strict limits for the maximum allowed levels (MAL) of AFB1 in groundnuts, milk, dried fruit and their products. For foods ready for retail sale the limit is 2 μg kg^{-1} for AFB1 (Van Egmond, 1995). Thus, regulatory and inspection agencies as well as industries need more robust methods for rapid, specific, sensitive, and in-field detection of AFB1 in foods and agricultural products to ensure food safety.

During the past few years, some well-established methodologies and analytical techniques have been studied for discrimination and quantization of AFB1 in many different foodstuffs, such as thin-layer chromatography (TLC), liquid chromatography (LC), immunoaffinity chromatography (IAC), high-performance liquid chromatography (HPLC) (Khayoon et al., 2010), liquid chromatography–mass spectrometry (LC–MS) (Nonaka et al., 2009), LC–MS/MS (Bacaloni et al., 2008), enzyme-linked immunosorbant assay (ELISA) (Li et al., 2009), electrochemical immunosensor (Piermarini et al., 2007) and so on. These methods are sensitive; however, more rapid, simple, and cost-effective approaches are still requested by the food industry. More recently optical biosensors coupled with gold nanoparticles (GNPs) provided a promising platform for this purpose based on their remarkably high extinction coefficient and strongly distance-dependent optical properties (Anker et al., 2008; Sepulveda et al., 2009; Storhoff et al., 2004). The color change in this case, which arises from the interparticle plasmon coupling during GNP aggregation or redispersion of an GNP aggregate (Zhao et al., 2008), is perhaps one of the most powerful and simple nanosensing

* Corresponding author at: Zhejiang University, College of Biosystems Engineering and Food Science, 866 Yuhangtang Rd., Hangzhou, China. Tel./fax: +86 571 88982885.
E-mail address: ybying@zju.edu.cn (Y. Ying).

0956-5663/$ - see front matter © 2013 Elsevier B.V. All rights reserved.
http://dx.doi.org/10.1016/j.bios.2013.03.048

methods available (Stewart et al., 2008). The methods demonstrated that sensitive detection of specific targets can be accomplished simply and rapidly without complex instrumentation. However, a big problem for this kind of materials is that spherical GNPs mostly used are not stable in high ionic environment or the existence of other impurities, resulting in undesirable GNP aggregation in complicated application environments (Zhang et al., 2012).

Gold nanorods (GNRs) have received a great deal of attentions due to their unique physical properties, and can provide several advantages over spherical nanoparticles for chemical and biological sensing. In particular, GNRs have a larger light absorption and scattering cross section in the surface plasmon resonance (SPR) wavelength region (Liu et al., 2008). The longitudinal absorption peak of GNRs, which can be tuned by adjusting their aspect ratio in the range of visible and near-infrared (NIR) wavelengths, is extremely sensitive to changes in the dielectric properties of the surroundings like the interparticle distances (Huang et al., 2006; Huang et al., 2009; Vigderman et al., 2012). Additionally, GNRs have a notable merit of high stability because of abundant cetyltrimethylammonium bromide (CTAB) either adsorbed on the surface or free in the solution, and can withstand high salt concentrations (above 0.5 M), providing promising applications of GNRs in detection of complicated real samples (He et al., 2008; Xu et al., 2012). However, most GNR-based optical biosensors have been reported for toxin immune sensing employed GNR-modified capture probes and oriented GNRs ensembles (Wang et al., 2010; Xu et al., 2011; Zhu et al., 2011) to improve the detection sensitivity, which made it not convenient and stable for biosensor fabrication. And previous application based on aggregation of GNRs were mostly reported by DNA hybridization (Darbha et al., 2008; Ma et al., 2010; Wang et al., 2012) which happened in salt environment, influenced by electrostatic interaction and undesirable aggregation.

In this research, we developed a simple and rapid optical biosensor based on competitive dispersion of GNRs, and only one-step detection procedure was needed for AFB1 determination. Specific antibodies employed as sensing probes were free in solution which induced a much better mixing and antibody-antigen interaction, and GNRs modified with AFB1–BSA conjugates were designed as competitors of the target analyte AFB1. GNRs aggregated after mixing with free antibodies against AFB1; while the existence of AFB1 molecules prevented aggregation as a result of binding with antibodies, which resulted in dispersion of GNRs in solution. This dispersion-dominated method could effectively reduce false results caused by undesirable aggregation in complicated application environments. Absorption intensity of UV–vis spectra served as the sensing indicator, while dynamic light scattering (DLS) measurement was used as another sensing tool. Furthermore, the testing result of AFB1 in real peanut samples was also reported using the dispersion-dominated method.

2. Materials and methods

2.1. Materials and reagents

CTAB, L-ascorbic acid, 11-mercaptoundecanoic acid (MUDA), sodium borohydride ($NaBH_4$), bovine serum albumin (BSA), AFB1–BSA conjugates and AFB1 were all purchased from Sigma-Aldrich (St Louis, MO, USA). Other mycotoxins used in the specificity evaluation including ochratoxin A (OTA), T-2 toxin, deoxynivalenol (DON) and zearalenone (ZON) were purchased from Fermentek (Jerusalem, Israel). Silver nitrate ($AgNO_3$) and hydrogen tetrachloroaurate (III) hydrate ($HAuCl_4 \cdot 3H_2O$) were purchased from Acros (Geel, Belgium). N-hydroxysuccinimide (NHS) and 1-(3-Dimethylaminopropyl)-3-ethylcarbodiimide hydrochloride (EDC) were purchased from Pierce (Rockford, USA). The monoclonal antibodies against AFB1 were purchased from IWC (Chair for Analytical Chemistry, Technical University of Munich, Germany). Other chemical reagents used were available commercially of high purity grade. Ultrapure water (18.2 MΩ cm, Millipore, Billerica, USA) was used in all tests.

2.2. Instrumentation

UV–vis absorption spectra were recorded by a SpectraMax M5 microtiter plate reader with Softmax® Pro Software (Molecular Devices, Sunnyvale, USA). The scanning wavelength was set from 400 to1000 nm for all measurements of GNRs. And 200 μL of the sample was added to each well to obtain its absorption spectrum. Transmission electron microscopy (TEM) images of GNRs were prepared by evaporating one drop of purified GNRs (10 μL) on a carbon-coated copper grid and acquired on a JEM-1230 transmission electron microscopy (JEOL, Tokyo, Japan). More than 200 particles were calculated for their size. The concentration of synthesized GNRs was determined by inductively coupled plasma mass spectrometry (ICP-MS, Agilent Technologies, Santa Clara, USA), combined with TEM images. Purified GNRs (10 mL) were digested by the addition of 2 mL of aqua regia (Orendorff and Murphy, 2006), and diluted for ICP-MS test. A minimum of three measurements were made for each sample.

The Zeta potential and DLS tests were performed using a Zetasizer Nano ZS90 (Malvern Instruments, Malvern, UK), which was operated under the following conditions: temperature 25 °C, detector angle 90°, incident laser wavelength 633 nm. And the sample was diluted to 2.0 mL with ultrapure water and measured three times. Raman spectra were collected with a DXR SmartRaman spectrometer (Thermo Scientific, Hudson, USA) at an excitation wavelength and power of 780 nm and 100 mW, respectively. The sample solutions with a volume of 30 μL were dried on glass substrates and the data presented was an average of three spectra taken at different locations.

2.3. Synthesis of GNRs

GNRs in aqueous solution were fabricated by a seed-mediated, Ag (I)-assisted growth procedure according to the previous reported methods (Liu and Guyot-Sionnest, 2005; Nikoobakht and El-Sayed, 2003; Sau and Murphy, 2004). First the seed solution was prepared. 5 mL of 0.5 mM $HAuCl_4$ was mixed with 5 mL of 0.2 M CTAB solution under constant stirring at 25 °C; then 0.6 mL of freshly prepared ice-cold 10 mM $NaBH_4$ was injected quickly into the solution, resulting in a brownish yellow solution; vigorous stirring of the seed solution was continued for at least 3 min for the complete decomposition of excess $NaBH_4$. After that, the seed solution was aged under gentle stirring at 25 °C for 1 h.

The growth solution was prepared by mixing 0.6 mL of 4 mM $AgNO_3$ with 40 mL of 0.1 M CTAB and 0.25 mL of 10 mM $HAuCl_4$. The resulting solution was acidified with 0.5 mL of 1 M HCl, followed by the addition of 0.32 mL of 0.1 M L-ascorbic acid with gentle stirring, which changed the growth solution from dark yellow to colorless. Then, 48 μL of gold seed was injected to the solution. And the growth reaction was slowly performed at 30 °C for 2 h. The GNRs were finally purified by centrifuging at 10,000 rpm for 15 min to remove excess reaction solution, and resuspensed in 0.005 M CTAB solution with a final volume of 40 mL.

2.4. Preparation of GNR-AFB1–BSA conjugates

The synthesized GNRs were covalent modified with AFB1–BSA conjugates (8–12 mol AFB1 per mol BSA) for the surface functionalization. 1.0 mL of 20 mM MUDA was added to 10 mL of purified GNRs in CTAB, and stirred mildly for 24 h under room temperature

(Yu and Irudayaraj, 2007a, 2007b), and the nanorods were centrifuged at 5000 rpm for 10 min and resuspensed in 1.0 mL of CTAB solution. Once the analkanethiol self-assembled monolayers (SAMs) were formed on the surface of GNRs, 0.2 mL mixture of 0.4 M EDC and 0.1 M NHS were added for activation of carboxyl group. Then, the GNRs were sonicated at 4 °C for 25 min, and purified by centrifuging at 5000 rpm for 10 min.

After activation, 1.0 mL of purified GNRs solution was added dropwise into 1.0 mL of 30 μg mL^{-1} AFB1–BSA conjugates, and kept oscillation under room temperature for 1 h. The resulting GNRs conjugates were collected by centrifugation at 5000 rpm for 10 min and washed twice with washing buffer (Phosphate-buffered saline solution containing 1% BSA). Finally, the GNR-AFB1–BSA conjugates were sonicated in CTAB solution for 10 min and stored at 4 °C. After each step of modification, 20 μL of functionalized GNRs was diluted to 200 μL and 2.0 mL for UV–vis and DLS measurements, respectively. The prepared GNR-AFB1–BSA conjugates were also characterized and confirmed by Raman spectroscopy and TEM analysis.

2.5. Optimization and detection procedures

To evaluate the detection performance with different concentrations of AFB1 antibody, antibodies in phosphate-buffered saline (PBS) solution with a concentration gradient from 5 to 30 μg mL^{-1} were mixed well with GNR-AFB1–BSA conjugates, and AFB1 standard solution (0 and 20 ng mL^{-1}), respectively; To study the performance with different adding volume of GNRs, GNR-AFB1–BSA conjugates from 20 to 80 μL were mixed with 40 μL of antibody (25 μg mL^{-1}) and AFB1 standard solution (0 and 20 ng mL^{-1}); To study the pH value of PBS on the performance of AFB1 detection, 40 μL of GNR-AFB1–BSA conjugates and 40 μL of AFB1 antibody (25 μg mL^{-1}) were mixed with AFB1 standard solution in three different pH buffers; 6.0, 7.0 and 8.0; To investigate the influence of reaction time on testing results, mixed solution with 40 μL of GNR-AFB1–BSA conjugates, antibody (25 μg mL^{-1}) and AFB1 standard solution were oscillated for 15 to 60 min, and diluted to 200 μL for UV–vis measurements.

To detect AFB1, 40 μL of GNR-AFB1–BSA conjugates were added to a 1.5-mL centrifuge tube, and mixed well with 40 μL of AFB1 in PBS at different concentrations: 0, 0.1, 0.5, 1.0, 2.0, 5.0, 10 and 20 ng mL^{-1}. Then 40 μL of 25 μg mL^{-1} AFB1 antibody was added and mixed well. The reaction solution was incubated under room temperature for 45 min. After incubation, each sample was diluted to 200 μL and used for UV–vis measurements and DLS analysis.

To evaluate the selectivity of the established approach, GNR-AFB1–BSA conjugates in the presence of OTA, T-2 toxin, DON, ZON and their mixtures with AFB1 were tested. The concentration of mycotoxins used and their mixtures with AFB1 in PBS buffer was all 20 ng mL^{-1}, which were determined by following the same sensing procedure for the target analyte AFB1.

2.6. Preparation of peanut samples

The fresh peanut samples purchased from a local market of agriculture products were finely ground with a laboratory mill, and 5 g of sample was placed in a 50-mL centrifuge tube. Then, 15 mL of methanol–water (80:20, v/v) containing 4% NaCl was added (Reiter et al., 2009; Zhang et al., 2011), and the sample was extracted by vortex mixing for 3 min. After centrifugation at 3500 rpm for 5 min at room temperature, 0.4 mL of supernatant was transferred to a 1.5-mL tube and diluted with 0.6 mL of pure water. The resulting solution was used as blank sample, and the spiked samples with different amounts of AFB1 were used as analytical samples.

3. Results and discussions

3.1. Strategy of GNR dispersion

The principle of AFB1 detection based on competitive dispersion of GNRs is present in Scheme 1. AFB1-BSA conjugates attach to the surface of GNRs initially to form GNR-AFB1–BSA conjugates as competitors, and then mixes well with AFB1 antibody and free AFB1 molecules. Free AFB1 molecules in sample solution compete with GNR-AFB1–BSA conjugates to combine with AFB1 antibody. Each monoclonal antibody produced by hybridoma technology which contains two light chains, has two antigen-binding sites found at the end of each light chain and can bind to two antigens (AFB1). Because the sequence of amino acids found at the end of each light chain of antibody can form a three-dimensional shape that is complementary to the shape of the antigen. And each AFB1–BSA conjugate used in this study had 8 to 12 AFB1 per BSA, which could bind to several antibodies. Thus it led to the aggregation of nanorods while the amount of free AFB1 was not enough. Fewer amounts of GNRs aggregate with the increase of AFB1 concentration, inducing GNR dispersion in solution as a result of competition. In another word, the dispersion of GNRs depends on the concentration of free AFB1 in solution, which could be used for AFB1 sensing.

3.2. Characterization of GNRs

GNRs with an aspect ratio of 3.1 (average length of 59 nm and diameter of 19 nm) were synthesized in 40 mL quantity and well dispersed in CTAB solution, according to TEM analysis of as-prepared GNRs displayed in Fig. 1(a) and S1. UV–vis absorption spectra of synthesized GNRs show a longitudinal plasmon resonance at 694 nm and a transverse plasmon resonance at 511 nm as displayed in Fig. 1(b). Zeta potential of prepared GNRs was +31.8 mV, induced by the positive layer of CTAB on the surface of nanorods. The average hydrodynamic size of GNRs in solution was 49.0 nm according to the DLS results. The weight of individual nanorods used in this study was calculated as 2.3×10^{-16} g based

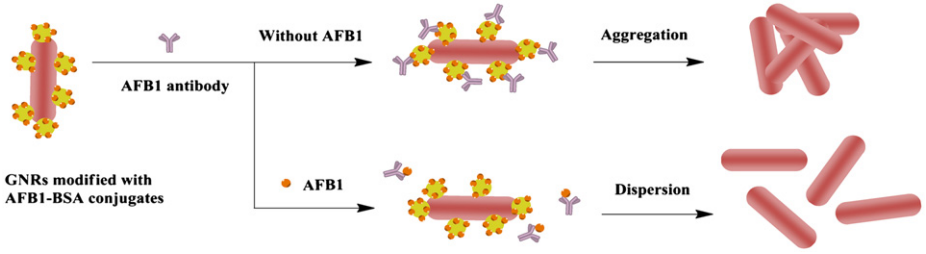

Scheme 1. Schematic illustration of AFB1 sensing based on competitive dispersion of GNRs.

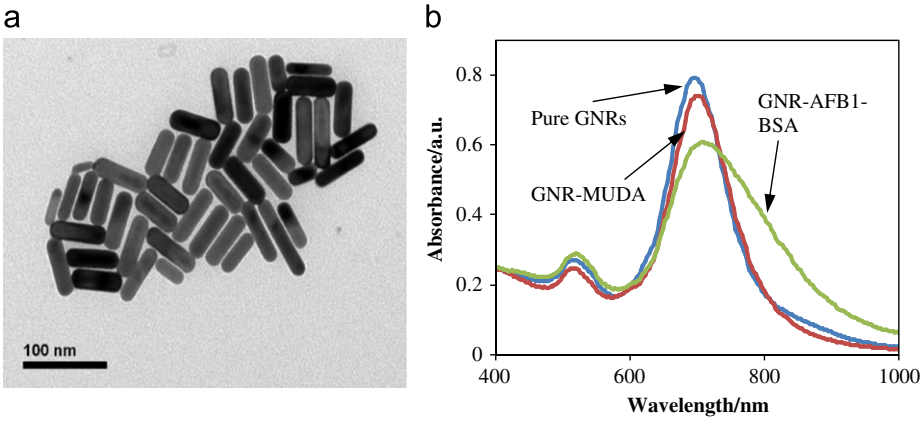

Fig. 1. (a) TEM images of synthesized GNRs; (b) UV–vis absorption spectra of synthesized GNRs, MUDA modified GNRs and GNR-AFB1–BSA conjugates. (For interpretation of the references to color in this figure legend, the reader is referred to the web version of this article.)

on TEM analysis by assuming GNRs are in *fcc* crystal structure. Since the total gold content in the purified GNR suspension was 21 mg L^{-1} (determined by ICP-MS), the concentration of synthesized GNRs was calculated as 0.16 nM (see Supporting Information).

Fig. 1(b) also shows the UV–vis absorption spectra of GNRs after MUDA modification and GNR-AFB1–BSA conjugates in a 5 mM CTAB solution. A red-shift of 6 nm and 15 nm in longitudinal peak was observed after modification of MUDA and AFB1–BSA conjugates in comparison to pure GNRs, with a red-shift of 3 nm and 6 nm in transverse peak. The shifts were most probably induced by the partially replacement of GNR surface from CTAB layer to AFB1–BSA conjugates. Absorption intensity of longitudinal peak versus the transverse peak, which was associated with the aspect ratio of GNRs, decreased from 2.92 to 2.17 after modification without peak broadening, indicating well modification of AFB1–BSA conjugates on the GNR surface without aggregation. The modification on the surface of GNRs was further characterized by Raman spectroscopy, without substrate interference of pure water compared with characterizations of other spectroscopy. As shown in Fig. S2, strongly enhanced Au–Br vibration at about 180 cm^{-1} in Raman spectrum of raw GNRs (Liao and Hafner, 2005) was lost after modification, suggesting CTAB present on the GNR surface was mostly replaced. MUDA were initially modified on the ends of GNRs, then on the sides. Since the attachment of CTAB to the ends of GNRs is weaker and as such this surface is more exposed and accessible to the chemical and biological linkers; CTAB on the sides of GNRs is harder to be replaced, because of their relatively large surface energy and stress (tension) compared to other surfaces of GNRs (Murphy et al., 2005).

Different from the CTAB layer, the AFB1–BSA conjugates in PBS buffer were negatively charged. As a result, zeta potential of GNRs decreased to +19.3 mV after amino modification. And the average size of GNR-AFB1–BSA conjugates increased to 55.8 nm. The approximate number of AFB1–BSA conjugates on the surface of individual GNR after modification could also be evaluated (see Supporting Information). It was most likely that, more conjugates were functionalized on the side surface than on the end surface, according to the aspect ratio change of GNRs using UV–vis analysis.

3.3. Optimization of the competitive dispersion

Fabricated GNR-AFB1–BSA conjugates were mixed with AFB antibody, and then competitively reacted with 0 ng mL^{-1} and 20 ng mL^{-1} of AFB1, respectively. Fig. S3 shows the DLS results of the two reaction samples. As expected, GNR-AFB1–BSA conjugates aggregated after incubation with AFB1 antibody without AFB1, but remained dispersed in the presence of AFB1. Hydrodynamic sizes of reacted GNRs were 776 nm and 80 nm while 0 ng mL^{-1} and 20 ng mL^{-1} of AFB1 was added, respectively. An obvious decrease of GNR aggregation was noticed with the addition of AFB1 in PBS buffer, which was in accordance with the TEM analysis as Fig. S4 shows. The AFB1 molecules competed with GNR-AFB1–BSA conjugates for binding to AFB1 antibodies, resulting in dispersion of GNRs. In addition, hydrodynamic size of conjugates under 100 nm was observed after reaction with 0 ng mL^{-1} of AFB1 from Fig. S3(a). Most probably, GNRs were not totally attached with AFB1–BSA conjugates during the modification process. Thus, non-functionalized GNRs capped with CTAB in the surface didn't participant in the test and remained in reaction solution, resulting in hydrodynamic size under 100 nm. GNR-AFB1–BSA conjugates non-aggregated after test which did not combine with AFB1 antibodies might also have contributed to it.

Further evidence of GNR aggregation was obtained with UV–vis spectroscopy. The absorption intensity of GNRs decreased after mixing with AFB1 antibody, caused by reduction of nanorods concentration in solution as a result of aggregation. However, after 20 ng mL^{-1} of AFB1 added, the intensity increased obviously in comparison with 0 ng mL^{-1} of AFB1. The influence of different conditions during competitive immune reaction between GNR-AFB1–BSA conjugates, free AFB1 molecules and AFB1 antibodies were investigated before quantitative analysis. GNR-AFB1–BSA conjugates were initially mixed with 20 and 0 ng mL^{-1} of AFB1 under different incubation conditions, respectively. And Fig. 2 shows their change of absorption intensity (ΔAbs) at 709 nm after incubation, which was used for optimization in the research.

The absorbance change (ΔAbs) of GNR-AFB1–BSA conjugates was increasing linearly after reaction with AFB1 antibodies with different concentrations from 5 to 25 μg mL^{-1}, and then decreasing from 25 to 30 μg mL^{-1} as shown in Fig. 2(a). It could be seen that GNRs in the presence of 25 μg mL^{-1} of AFB1 antibodies showed the strongest ΔAbs signal. Most likely, the aggregation of GNRs increased initially and then reached saturation with the increase of antibody concentration. Then the GNR-AFB1–BSA conjugates (volume of 20 μL, 40 μL, 60 μL and 80 μL were included) were optimized by mixing with 40 μL, 25 μg mL^{-1} of AFB1 antibodies. It is indicated from Fig. 2(b) that the optimal volume of GNR-AFB1–BSA conjugates was 40 μL for quantitative analysis. In another word, optimal adding ratio of GNR-AFB1–BSA conjugates versus the target analyte AFB1 was 1:1.

GNRs and GNR-AFB1–BSA conjugates capped with CTAB layer were positively charged (Murphy et al., 2010). Thus, it is possible to be influenced by nonspecific adsorption, especially electrostatic

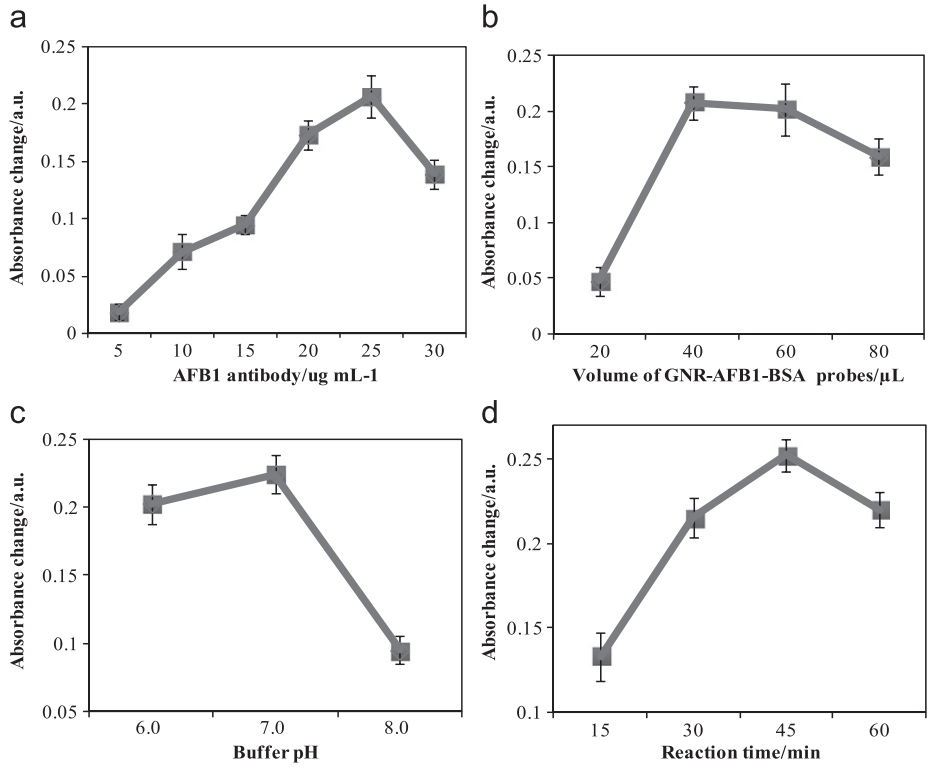

Fig. 2. Optimization of competitive dispersion according to absorbance change (ΔAbs) of GNR-AFB1–BSA conjugates after reaction with 0 and 20 ng mL^{-1} of AFB1: (a) the concentration of AFB1 antibody; (b) the adding volume of GNR-AFB1–BSA conjugates; (c) pH of buffer solution; and (d) reaction time.

interaction. AFB1 antibodies were negative charged in buffers with a pH greater than 7.0, since the isoelectric point of AFB1 antibodies is in the range of 6.0–7.0. Proteins such as AFB1 antibody negatively charged may be easily and directly adsorbed onto the GNR surface. To study the nonspecific adsorption of antibody to GNR, the influences of pH values of PBS buffer were investigated. Standard samples in PBS buffer with different pH values (6.0, 7.0, and 8.0) were tested. As shown in Fig. 2(c), the obtained ΔAbs values when antibodies (pH=6.0) are positive charged and slight negative charged (pH=7.0) were not significantly different ($<9.1\%$). It indicates that the nonspecific adsorption was still suppressed at pH 7.0. But an obvious decreases of ΔAbs indicated the significant nonspecific adsorption happened at pH 8.0. Thus PBS buffer with pH 7.0 was selected for following quantitative analysis. Under the above optimal conditions, the strongest ΔAbs signal was obtained when reaction process lasted for 45 min according to Fig. 2(d).

3.4. Analytical performance

After optimization, fabricated GNR-AFB1–BSA conjugates were mixed with different concentrations of AFB1 in PBS (0, 0.1, 0.5, 1.0, 2.0, 5.0, 10 and 20 ng mL^{-1}) for quantitative analysis. Negative sample of PBS buffer was measured as the blank. Fig. 3(a) shows the UV–vis absorption spectra of GNRs after reaction. It can be observed that a new longitudinal peak appeared at 850 nm and original longitudinal peak almost disappeared while AFB1 concentration ranged from 0 to 5 ng mL^{-1}. Obvious aggregation of GNRs was indicated, together with significant band-broadening. However, while AFB1 concentration was greater than 5 ng mL^{-1}, original longitudinal peak of GNRs at 709 nm appeared and remained as the predominant longitudinal peak compared with that at 850 nm, which was induced by GNR dispersion after antibodies interaction with AFB1 rather than GNR-AFB1–BSA conjugates. In addition, the absorption intensity of GNRs at 709 nm increased with increasing of AFB1 concentration in the range of 0–20 ng mL^{-1} caused by change of interparticle distances and increase of dispersed nanorods in solution.

The sensitivity of this GNR based biosensing system was determined in this work. As shown in Fig. 3(b), calibration plots represented the absorbance change of GNR-AFB1–BSA conjugates at 709 nm from the blank. The data were linearly correlated with equation $\Delta Abs = 0.013C_{AFB1} + 0.034$ with a correlation coefficient of 0.99 in the concentration range of 0.5 to 20 ng mL^{-1}. And the limit of detection (LOD) was calculated to be 0.16 ng mL^{-1} for AFB1 based on three times of signal-to-noise ratio, which could meet the need for detection of the allowed AFB1 in foods ready for retail sale according to the European Commission standards. Although the new method described in the present study has no advantage in sensitivity over other immunoassays for AFB1, such as commonly used plate-ELISA method (LOD: 0.01–10 ng mL^{-1}) and electrochemical immunosensors with high sensitivity (LOD: 0.01–0.4 ng mL^{-1}) (Li et al., 2009). The proposed approach is rapid without additional enzyme-labeled antibody or signal enhancement, and is simple to operate.

Moreover, the average hydrodynamic sizes of GNRs after reaction with different concentrations of AFB1 were tested by DLS measurement, which is a powerful tool for nanoparticle bioconjugation and biomolecular binding studies (Jans et al., 2009). With increasing of the AFB1 concentration, fewer GNRs aggregated in solution resulting in decrease of GNR sizes and gradually reached saturation as shown in Fig. S5(a), which was in accordance with the results of UV–vis spectroscopy. And the calibration curve between AFB1 concentration and DLS results was shown in Fig. S5(b).

To evaluate the selectivity of the established approach, upconversion absorbance signal of dispersed GNRs after incubation caused by the binding of OTA, T-2, DON, and ZON were analyzed, respectively. As a result, it was observed (Fig. 4) that the response induced by other mycotoxins was much lower, no more than 4.2%

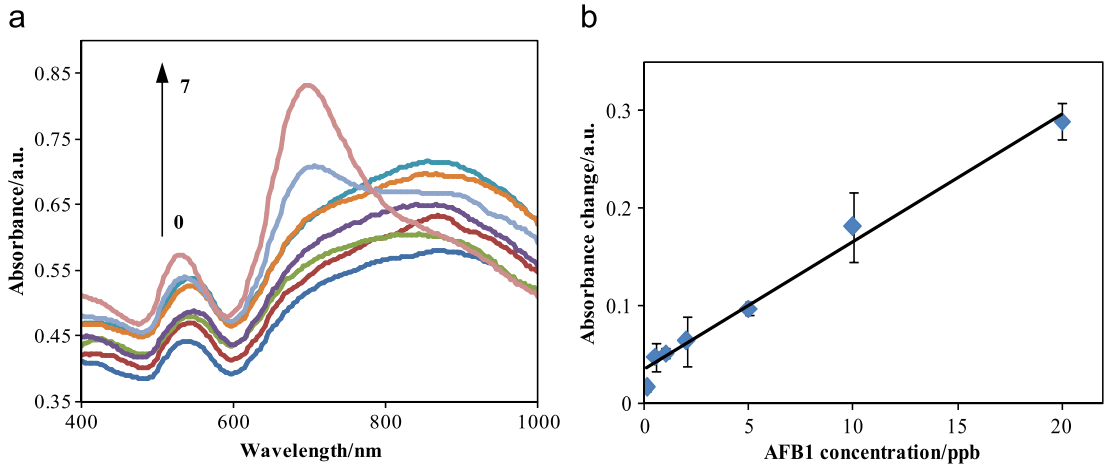

Fig. 3. Determination results of AFB1 in PBS: (a) UV–vis absorption spectra of GNR-AFB1–BSA conjugates after reaction with different concentrations of AFB1 (from sample 0 to 7: 0, 0.1, 0.5, 1.0, 2.0, 5.0, 10 and 20 ng mL^{-1}); (b) the relationship between absorbance changes of GNRs at 709 nm and AFB1 concentration.

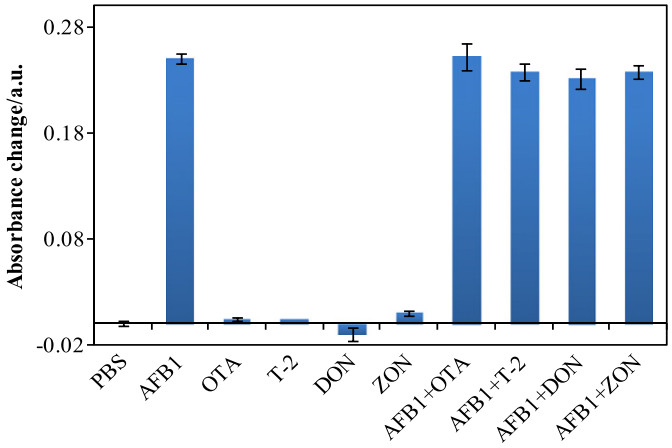

Fig. 4. The selectivity of AFB1 determination: absorbance of GNR-AFB1–BSA conjugates after reaction. And the concentration of AFB1, OTA, T-2, DON, ZON and their mixtures in PBS buffer was 20 ng mL^{-1}.

Table 1
Results of the proposed approach for peanut samples based on competitive dispersion of GNRs.

Spiked level (ng mL^{-1})	Detected concentration (ng mL^{-1})	RSD (ng mL^{-1})	Recovery (%)
0.5	0.471	0.1440	94.2
1	1.173	0.2992	117.3
5	5.219	0.5808	104.4
10	10.515	0.7071	105.2
20	19.496	1.3435	97.5

compared to the response induced by the target analyte AFB1 indicating the high selectivity of this biosensor. And the signal variations caused by the presence of interfering mycotoxins in foods was lower than 7.5% of AFB1 signal, suggesting a negligible impact on the detection.

3.5. Analytical application

The feasibility of biosensor based on GNR dispersion for possible application was evaluated by analysis of peanut samples. A non-artificially contaminated peanut sample was used as the negative control. The prepared blank and spiked samples were tested by replacing AFB1 standard samples as mentioned above. And the concentration of AFB1 in peanut samples was determined from the calibration curve. The testing results are summarized in Table 1. Satisfactory recoveries as shown in Table 1, ranging from 94.2% to 117.3% were obtained, indicating acceptable accuracy of the proposed detection sensor for AFB1 in real samples. This analysis demonstrated that the established biosensing system could be applied for AFB1 determination in real agriculture products.

4. Conclusions

In summary, a promising one-step optical biosensing approach based on competitive dispersion of GNRs was demonstrated for AFB1 analysis. AFB1 in PBS solution could be detected at low concentrations linearly ranged from 0.5 to 20 ng mL^{-1}, based on the changes in absorption intensity of UV–vis spectra at 709 nm and the size of GNRs. The whole test from taking samples to final measurement could be completed within 45 min. And the feasibility of this approach for AFB1 detection was also demonstrated in artificially contaminated peanut samples. The success of the present report for AFB1 detection indicates the potential of GNRs as a biosensing platform to be put into practice toward simple, rapid, and specific in-field screening of food safety.

Acknowledgments

This work was financially supported by the National Natural Science Foundation of China (No. 30825027). The authors appreciate Dr. Yingyue Zhu (Jiangnan University, China) for helpful discussions. And the authors are also thankful to the 985-Institute of Agrobiology and Environmental Sciences at Zhejiang University, for providing convenience in use of their facilities and equipments.

Appendix A. Supporting information

Supplementary data associated with this article can be found in the online version at http://dx.doi.org/10.1016/j.bios.2013.03.048.

References

Anker, J.N., Hall, W.P., Lyandres, O., Shah, N.C., Zhao, J., Van Duyne, R.P., 2008. Nature Materials 7, 442–453.
Bacaloni, A., Cavaliere, C., Cucci, F., Foglia, P., Samperi, R., Lagana, A., 2008. Journal of Chromatography A 1179, 182–189.

Darbha, G.K., Rai, U.S., Singh, A.K., Ray, P.C., 2008. Chemistry—A European Journal 14, 3896–3903.
Delmulle, B.S., De Saeger, S.M.D.G., Sibanda, L., Barna-Vetro, I., Van Peteghem, C.H., 2005. Journal of Agricultural and Food Chemistry 53, 3364–3368.
He, W., Huang, C.Z., Li, Y.F., Xie, J.P., Yang, R.G., Zhou, P.F., Wang, J., 2008. Analytical Chemistry 80, 8424–8430.
Huang, X., El-Sayed, I.H., Qian, W., El-Sayed, M.A., 2006. Journal of the American Chemical Society 128, 2115–2120.
Huang, X.H., Neretina, S., El-Sayed, M.A., 2009. Advanced Materials 21, 4880–4910.
Jans, H., Liu, X., Austin, L., Maes, G., Huo, Q., 2009. Analytical Chemistry 81, 9425–9432.
Khayoon, W.S., Saad, B., Yan, C.B., Hashim, N.H., Ali, A.S.M., Salleh, M.I., Salleh, B., 2010. Food Chemistry 118, 882–886.
Lee, N.A., Wang, S., Allan, R.D., Kennedy, I.R., 2004. Journal of Agricultural and Food Chemistry 52, 2746–2755.
Li, P., Zhang, Q., Zhang, W., 2009. TrAC Trends in Analytical Chemistry 28, 1115–1126.
Liao, H., Hafner, J.H., 2005. Chemistry of Materials 17, 4636–4641.
Liu, M.Z., Guyot-Sionnest, P., 2005. Journal of Physical Chemistry B 109, 22192–22200.
Liu, X., Dai, Q., Austin, L., Coutts, J., Knowles, G., Zou, J., Chen, H., Huo, Q., 2008. Journal of the American Chemical Society 130, 2780–2782.
Ma, Z., Tian, L., Wang, T., Wang, C., 2010. Analytica Chimica Acta 673, 179–184.
Murphy, C.J., San, T.K., Gole, A.M., Orendorff, C.J., Gao, J.X., Gou, L., Hunyadi, S.E., Li, T., 2005. Journal of Physical Chemistry B 109, 13857–13870.
Murphy, C.J., Thompson, L.B., Alkilany, A.M., Sisco, P.N., Boulos, S.P., Sivapalan, S.T., Yang, J.A., Chernak, D.J., Huang, J., 2010. Journal of Physical Chemistry Letters 1, 2867–2875.
Nikoobakht, B., El-Sayed, M.A., 2003. Chemistry of Materials 15, 1957–1962.
Nonaka, Y., Saito, K., Hanioka, N., Narimatsu, S., Kataoka, H., 2009. Journal of Chromatography A 1216, 4416–4422.
Orendorff, C.J., Murphy, C.J., 2006. Journal of Physical Chemistry B 110, 3990–3994.
Piermarini, S., Micheli, L., Ammida, N.H.S., Palleschi, G., Moscone, D., 2007. Biosensors and Bioelectronics 22, 1434–1440.
Reiter, E.V., Cichna-Markl, M., Chung, D.-H., Zentek, J., Razzazi-Fazeli, E., 2009. Journal of Separation Science 32, 1729–1739.
Sau, T.K., Murphy, C.J., 2004. Journal of the American Chemical Society 126, 8648–8649.
Sepulveda, B., Angelome, P.C., Lechuga, L.M., Liz-Marzan, L.M., 2009. Nano Today 4, 244–251.
Stewart, M.E., Anderton, C.R., Thompson, L.B., Maria, J., Gray, S.K., Rogers, J.A., Nuzzo, R.G., 2008. Chemical Reviews 108, 494–521.
Storhoff, J.J., Lucas, A.D., Garimella, V., Bao, Y.P., Muller, U.R., 2004. Nature Biotechnology 22, 883–887.
Van Egmond, H.P., 1995. Food Additives and Contaminants 12, 321–330.
Vigderman, L., Khanal, B.P., Zubarev, E.R., 2012. Advanced Materials 24, 4811–4841.
Wang, L., Zhu, Y., Xu, L., Chen, W., Kuang, H., Liu, L., Agarwal, A., Xu, C., Kotov, N.A., 2010. Angewandte Chemie International Edition 49, 5472–5475.
Wang, X., Li, Y., Wang, J., Wang, Q., Xu, L., Du, J., Yan, S., Zhou, Y., Fu, Q., Wang, Y., Zhan, L., 2012. Analyst 137, 4267–4273.
Williams, J.H., Phillips, T.D., Jolly, P.E., Stiles, J.K., Jolly, C.M., Aggarwal, D., 2004. American Journal of Clinical Nutrition 80, 1106–1122.
Xu, L., Kuang, H., Wang, L., Xu, C., 2011. Journal of Materials Chemistry 21, 16759–16782.
Xu, X., Ying, Y., Li, Y., 2012. Sensors and Actuators B: Chemical 175, 194–200.
Yu, C., Irudayaraj, J., 2007a. Biophysical Journal 93, 3684–3692.
Yu, C.X., Irudayaraj, J., 2007b. Analytical Chemistry 79, 572–579.
Zhang, D., Li, P., Zhang, Q., Zhang, W., 2011. Biosensors and Bioelectronics 26, 2877–2882.
Zhang, D., Li, P., Zhang, Q., Zhang, W., Huang, Y., Ding, X., Jiang, J., 2009. Analytica Chimica Acta 636, 63–69.
Zhang, M., Qing, G., Xiong, C., Cui, R., Pang, D.-W., Sun, T., 2012. Advanced Materials 25, 749–754.
Zhao, W., Brook, M.A., Li, Y., 2008. ChemBioChem 9, 2363–2371.
Zhu, Y., Qu, C., Kuang, H., Xu, L., Liu, L., Hua, Y., Wang, L., Xu, C., 2011. Biosensors and Bioelectronics 26, 4387–4392.